Proceedings of the ASME 2010 Pressure Vessels & Piping Division / K-PVP Conference
PVP2010
July 18-22, 2010, Bellevue, Washington, USA

PVP2010-25833

DIAPHRAGM CLOSURE ANALYSIS USING NONLINEAR FEA AND CFD

Sean McGuffie
Porter McGuffie, Inc.
Lawrence, KS, USA
785-856-7575 x102
sean@pm-engr.com

Mike Porter
Dynamic Analysis
Lawrence, KS, USA
785-843-3558
mike@dynamicanalysis.com

Dennis Martens
Porter McGuffie, Inc.
Lawrence, KS, USA
913-484-3868
martensdh@pm-engr.com

ABSTRACT

In the previous work PVP2006-93731 "Reinvestigation of Heat Exchanger Flange Leak" (Porter [1]), a series of finite element (FE) models were constructed of a heat exchanger flange. Current FE capabilities were used to further elucidate the reasons for the flange's leakage in-service, reported in a 1994 paper (Porter [2]). The flange leakage was primarily caused by differential thermal expansion causing yield in the flange bolts and gasket scuffing. Correcting the leakage required the implementation of a weld ring gasket.

A similar service exchanger was later designed to eliminate the critical differential thermal expansions. This exchanger employed a diaphragm closure method to eliminate the possibility of gasket leakage. This design included an internal pass partition arrangement such that the end closure flanges were exposed to a single process fluid temperature. In the authors' experience, typically the exchanger vendor provides proprietary calculations verifying the serviceability of the closure design. This prompted the question, "What analysis methodology would be required for an engineer to qualify or verify the design of a welded diaphragm closure configuration?"

The authors have used a thorough methodology for the analysis of a diaphragm closure. This was used for verification of the design suitability for design temperature gradients and related thermal expansion. To conduct the analysis, the authors performed a series of computational fluid dynamics (CFD) and non-linear FE analyses on a representative diaphragm closure geometry (under specific service conditions) to determine the closure's capability to withstand the design load cases. This paper serves to demonstrate how such analyses can be used to qualify a diaphragm closure's suitability for a specific service.

It should be noted that this paper does not represent a complete analysis of a diaphragm closure. Code (ASME [3]) specifies all procedures that shall be employed. The procedures under investigation were applied to the 2 cases analyzed. Complete engineering of the closure may require the analysis of additional cases.

INTRODUCTION

As reported in [1] and [2], the classic gasket type flanged exchanger closure is not satisfactory for some services. One such instance is where differential expansion resulting in yielding of the bolting and scuffing of the gasket surface can occur. For services where leakage is not tolerable, it is necessary to address the thermal driven displacements to provide suitable gasket sealing conditions. However in certain services, it is desirable to provide a welded closure to eliminate the potential for leakage. The use of diaphragm closure may be utilized. The design analysis of a diaphragm closure is not addressed by the ASME BPVC Section VIII (ASME [4]) or ASME Code for Process Piping B 31.3. (ASME [5]) Unlike standardized gasket dimensions provided in ASME B 16.20 (ASME [6]), diaphragm closure standardized dimensions are not available.

Diaphragm closures are designed to accommodate either standard flange dimensions or specially designed

Copyright © 2010 by ASME

flanges. A typical diaphragm closure design for a heat exchanger channel is shown in Figure 1.

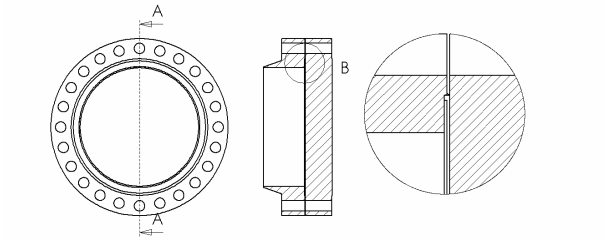

FIGURE 1 – SCHEMATIC OF DIAPHRAGM SEAL

The representative diaphragm closure design selected for the analysis reported in this technical paper is typical of diaphragm closures that have been successfully used in the refining and chemical industry for critical services.

The representative diaphragm closure analyzed in this paper utilizes the standardized dimensions for a 48" Class 900 Series A flange, per ASME B 16.47 (ASME [7]). The diaphragm dimensions are indicated in Figure 2.

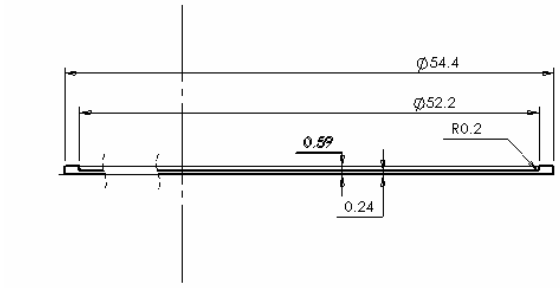

FIGURE 2 – DIAPHRAGM DIMENSIONS USED IN ANALYSIS

PROBLEM DESCRIPTION

Figure 3 contains a 3-dimensional cross section of the diaphragm closure under consideration. As can be seen from the figure, the pressure load due to the bolt clamping force imparted to the back of the diaphragm by the blind flange (BF) serves to form a metal–to-metal seal of the diaphragm against the channel weld neck flange (WNF). Additionally, there is a seal weld between the WNF and the diaphragm around the diaphragm's outer perimeter.

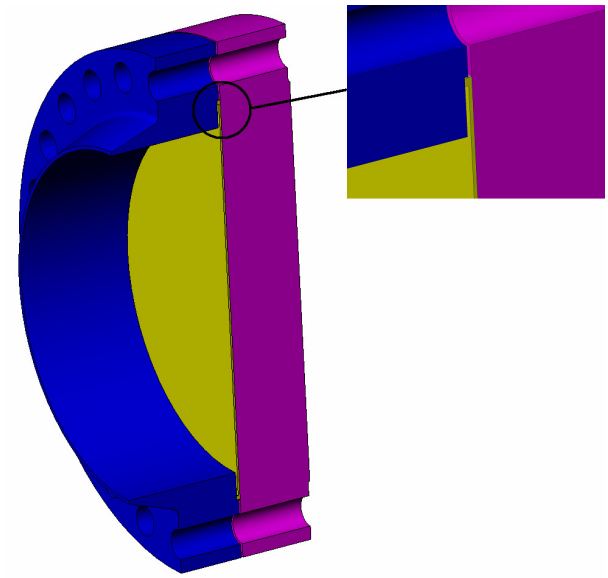

FIGURE 3 – 3-DIMENSIONAL REPRESENTATION OF DIAPHRAGM SEAL

Most of the exchanger components are constructed of carbon steel (516-70) with a stainless steel weld overlay. As carbon steel is not suitable for the operating environment, the diaphragm and weld materials are 347 stainless steel. For these analyses, the weld overlay was not considered.

The internal surfaces of the exchanger are exposed to hydrocarbon service at a nominal temperature of 750 °F and pressure of 1350 psi. By design, the diaphragm does not resist any of the operational pressure end load due to the presence of the BF. As is readily apparent, both flanges have considerable thermal mass compared to the diaphragm, and could be partially insulated or not insulated. Therefore, it is reasonable to expect that the diaphragm may heat up or cool down much quicker than the flanges. This differential heating, combined with dissimilar materials and thermal expansion coefficients between the flanges and diaphragm would be expected to result in differential thermal expansion conditions in the exchanger components.

Section VIII Div. 1 Paragraph UG22 LOADINGS [4] requires all appropriate loadings to be considered in the design of the diaphragm closure, including analysis of the flanges' temperature gradients and differential thermal expansions as studied in [1], as well as all mechanical loads imparted during service

SOLVING THE PROBLEM

The stresses due to the thermal and mechanical loads on the diaphragm and on the closure weld must be characterized to allow for qualification of the design.

To characterize the stresses due to the operational loads, CFD and FE models were used. As detailed in the **CFD MODEL** Section, analyses were used to address the fluid heat transfer characteristics and to

Copyright © 2010 by ASME

provide the necessary input for the FE analysis. The FE model was used to perform transient thermal analyses under a wide variety of conditions. The temperatures from the extreme differential expansion and loading cases analyzed were transferred to structural models to determine the operational stresses. Several thermal and load transfer cases were considered.

Using plastic analysis, the stresses from the analyses were then evaluated to assess the permanent strain of the structure. Elastic analysis was used to support the procedures specified in ASME Section VIII, Div. 2, Part 5.5.3 Fatigue Assessment – Elastic Stress Analysis and Equivalent Stresses (ASME [8]).

CFD MODEL

As shown in Figure 3, there is a small passage exposed to the exchanger process fluid between the diaphragm and the WNF. As differential expansion was of concern in the structural analysis, the decision was made to use a CFD model solved in Star-CCM+ (CD-Adapco [9]) to calculate the flow field and the convection coefficients on various locations within the design. This was deemed important due to the passages where the coefficient should be significantly reduced. The CFD model only considered the local area around the diaphragm closure seal, as shown in Figure 4's exploded view.

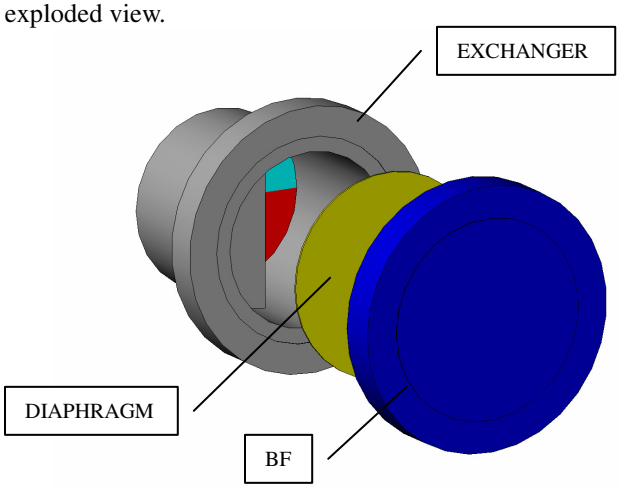

FIGURE 4 – EXPLODED VIEW OF EXCHANGER INTERNALS

In this figure, the protrusion on the left side of the exchanger represents proprietary exchanger design features for the internal pass partitions. The exchanger has two U-tube passes. The hydrocarbon enters the inlet nozzle, passes through the lower U-tube and exits the first pass on the red face. Turbulent flow then exists in the open passageway where the fluid eventually turns and enters the second pass on the blue face.

A CFD model was constructed representing the flow space within Figure 4, the exchanger, insulation, BF and diaphragm. Figures 5 and 6 show the geometry of the CFD model.

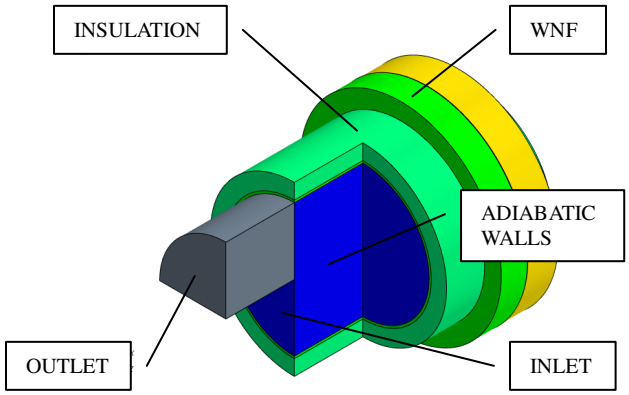

FIGURE 5 – CFD MODEL USED FOR ANALYSIS, FRONT VIEW

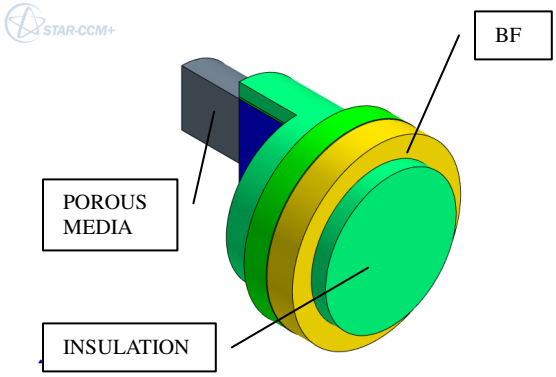

FIGURE 6 – CFD MODEL USED FOR ANALYSIS, REAR VIEW

An inlet was defined at the exit of the first pass and an outlet was defined at the entrance to the second pass. To represent the resistance offered by the tubes - required to properly calculate the exit flow field, a porous media was included in the model at the exit. This media represented the first two feet of the tubes. The porosity values in the orthogonal directions were set to a very high value so that flow in these directions did not exist in the tube field.

The model was constructed using a hexahedral mesh with near wall refinement and contained approximately 960,000 cells. Figure 7 contains an image of the model.

Copyright © 2010 by ASME

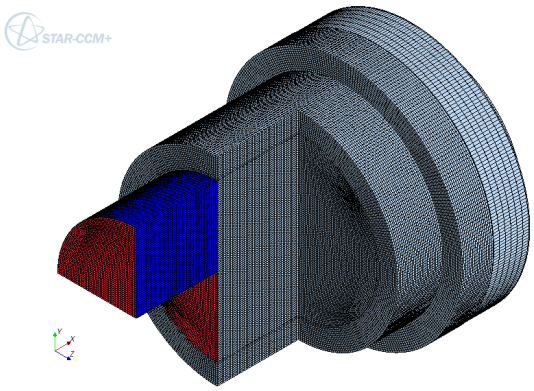

FIGURE 7 – MESH USED FOR CFD ANALYSIS

The working fluid within the model was defined as dodecane. This was the heaviest hydrocarbon with a complete set of properties for fluid analysis documented in the public domain (CD-Adapco [10]). The exchanger and BF in the model were modeled as carbon steel; the diaphragm and weld were modeled as stainless steel; and the insulating blankets were modeled as ZIRCAR fiber blanket. Table 1 contains the relevant material properties for the fluid and steel components.

Material	*Property*	*English*	*Units*	*SI*	*Units*
Dodecane	Density	0.027	lb/in^3	745.76	kg/m^3
	Viscosity	1.38	cP	1.38	cP
	Thermal Conductivity	0.078	BTU/hr*ft^2*F	0.1349	W/m*K
Carbon Steel	Thermal Conductivity	36.9	BTU/hr*ft^2*F	63.9	W/m*K
Stainless Steel	Thermal Conductivity	8.7	BTU/hr*ft^2*F	15.1	W/m*K

TABLE 1 – MATERIAL PROPERTIES USED FOR CFD ANALYSIS

Figure 8 contains the line fit used for the ZIRCAR properties (MatWeb [11]), implemented through a field function.

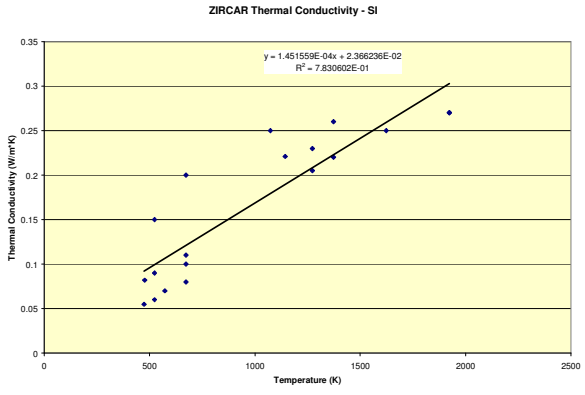

FIGURE 8 – LINE FIT FOR ZIRCAR THERMAL CONDUCTIVITY

Convection on the external (atmospheric) surfaces was modeled through the use of a convection coefficient of 3.2 BTU/hr*ft^2*°F (18 W/m^2*K) applied to the exposed faces with a bulk temperature of 70 °F (21 °C). On the faces between the flanges, the coefficient was lowered to 0.64 BTU/hr*ft^2*°F (3.6 W/m^2*K).

To perform the analysis, an inlet velocity of 32.8 ft/s (10 m/s) was applied at the inlet. The outlet was defined as an Outflow boundary condition. Initially the velocity field within the fluid was solved using a steady-state analysis. Figure 9 shows streamlines colored by velocity from this analysis.

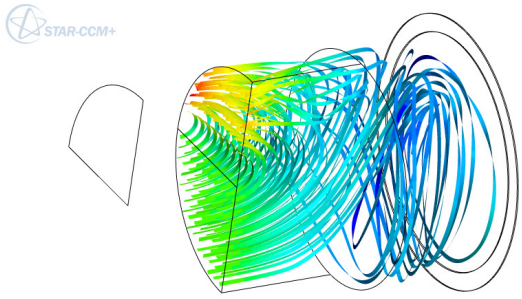

FIGURE 9 – FLOW STREAMLINES COLORED BY VELOCITY MAGNITUDE

As can be seen from the figure, there is highly turbulent flow in the region of the WNF and the diaphragm. This should serve to increase the effective heat transfer at these locations. After a converged flow solution had been achieved, the energy equation was activated and the flow solution was frozen. Solution was allowed to proceed until the energy equation had converged.

Four regions were defined on the interfaces between the fluid and the exchanger components where the average convection coefficient was queried from the analysis. Figures 10 and 11 show the locations, with call-outs.

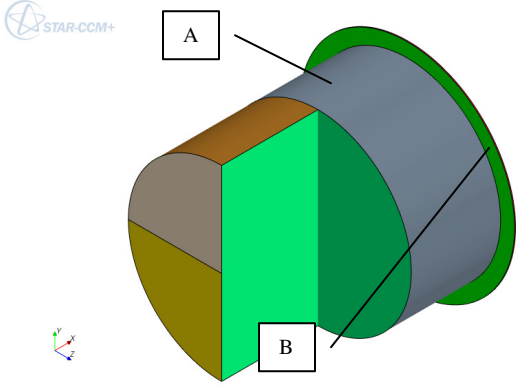

FIGURE 10 – LOCATION CALLOUTS FOR QUERIED CFD VALUES, FRONT VIEW

Copyright © 2010 by ASME

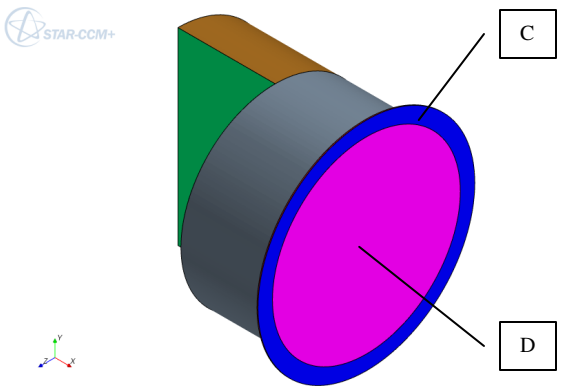

FIGURE 11 – LOCATION CALLOUTS FOR QUERIED CFD VALUES, REAR VIEW

The bullet points below give a description of each location:

A. The area of the WNF exposed to direct hydrocarbon flow
B. The area of the WNF exposed to hydrocarbon flow in the small passage
C. The area of the diaphragm exposed to hydrocarbon flow in the small passage
D. The area of the diaphragm exposed to direct hydrocarbon flow

Table 2 contains the approximate queried values from the analysis. The queried values are well within reasonable ranges for a liquid hydrocarbon service (Hodge [12]).

Location	hi, BTU/hr*ft^2*F	hi, W/m^2*K
A	370	2100
B	190	1080
C	190	1080
D	420	2380

TABLE 2 – QUERIED CFD CONVECTION COEFFICIENTS

FEA MODEL

A finite element model was used to categorize the stresses in the assembly. The FE model was used to perform both transient thermal analyses on the assembly and stress analyses. The model was used for the transient thermal analyses so the temperatures could be transferred on a node–by-node basis to the structural model. The following assumptions were associated with the FE analysis:

1) The clamping force provided by the bolts was invariant around the perimeter of the flange
2) Thermal variation around the flange's perimeter was negligible
3) The loss in flange structural strength and the stress variation effect in the diaphragm area under study, due to the bolt holes, was negligible
4) At any radius from the centerline, contact between the BF and diaphragm was consistent

When incorporating these assumptions, it was decided to use an axisymmetric model for the analyses. The use of an axisymmetric model would allow for a wide variety of analysis parameters to be quickly studied to determine their effect on the results. As contact and possibly plasticity would need to be studied during the analyses a series of test models were used to determine a mesh density that minimized mesh discretization errors while minimizing the model size. Figure 12 contains an image of the final FE model used for the analyses.

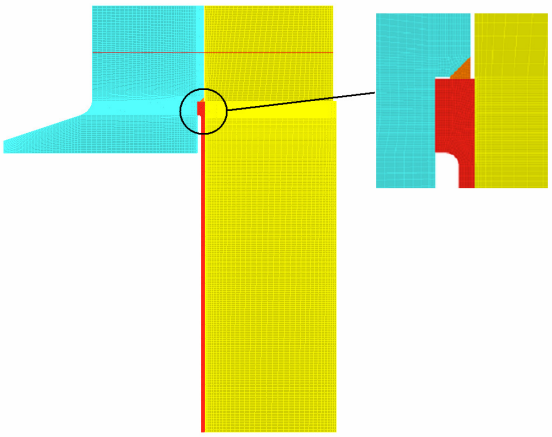

FIGURE 12 – FE MODEL USED FOR ANALYSIS

The flanges, diaphragm and weld were modeled using 2-dimensional axisymmetric elements. The bolts and bolt spider were represented using beam elements. The bolts were given a diameter so that the bolt area in the model matched the bolt area in 1 radian of the flange, or 7.8 in (0.2 m).

All analyses were performed using Algor v. 23 (Algor [13]).

Transient Thermal Analysis

To perform the transient thermal analysis the convection coefficients determined during the **CFD MODEL** Section were applied to their corresponding locations on the axisymmetric model. The same external convection coefficients used during the CFD analysis were applied to the exposed faces of the model. Where insulation was present, the convection coefficient was set to 1/200th of the standard coefficient. Thermal contact, using surface–to-surface contact elements, was included between the WNF and

Copyright © 2010 by ASME

diaphragm and between the BF and diaphragm at locations where they interacted.

Two heating rates were considered during the analyses, 50 °F/hr and 150 °F/hr, with an initial temperature of 70 °F. As previously mentioned, a final temperature of 750 °F was used. The temperature ramps were implemented by modifying the internal bulk temperature using linear functions. As there is no standard in industry as to whether the BF will be insulated, cases were run for both insulated and uninsulated BFs. The insulation did not extend to cover the stud bolts. Typically, industry does not insulate stud bolts, but rather exposes these to the ambient environment. A literature search (GE [14]) produced three possible values for the contact resistance between the BF and diaphragm, depending on the surface finish, contact pressure, and material types:

- 0.000195 hr-ft^2-°F/BTU (3.43 x 10^{-5} m^2*K/W),
- 0.000442 hr-ft^2-°F/BTU (7.78 10^{-5} m^2*K/W), and
- 0.000771 hr-ft^2-°F/BTU (1.36 10^{-6} m^2*K/W)

As no better information was available, all three values were examined during the analyses. Table 3 shows the run matrices used for the transient thermal analyses.

Master Case	*Heating Rate (deg/hr)*	*Contact Resistance (hr-ft2-F/BTU)*
No Insulation	50	None
	50	0.000195
	50	0.000442
	50	0.000771
	150	None
	150	0.000195
	150	0.000442
	150	0.000771
Insulation	50	None
	50	0.000195
	50	0.000442
	50	0.000771
	150	None
	150	0.000195
	150	0.000442
	150	0.000771

TABLE 3 – RUN MATRIX FOR TRANSIENT THERMAL FE RUNS

Figure 13 contains the temperature-dependent thermal conductivities applied to the model from ASME BPVC Section II, Table TCD (ASME [15]).

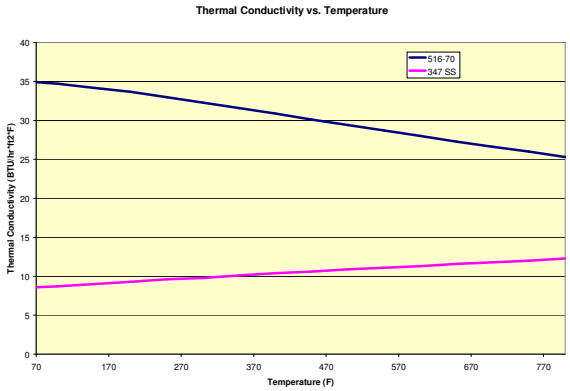

FIGURE 13 – TEMPERATURE DEPENDENT THERMAL CONDUCTIVITIES

The average temperature versus time for three model components - the WNF, BF and diaphragm - were output from each analysis. These mean temperatures were then used to calculate the linear growth of each component at the time step using the mean thermal expansion coefficient taken from Table TE-1 [10]. Figure 14 shows the differential displacements between components at the centerline of the diaphragm sealing face versus bulk temperature (normalization for difference in heating time scales for warm-up rate) for the 50 °F/hr heat up case with insulation.

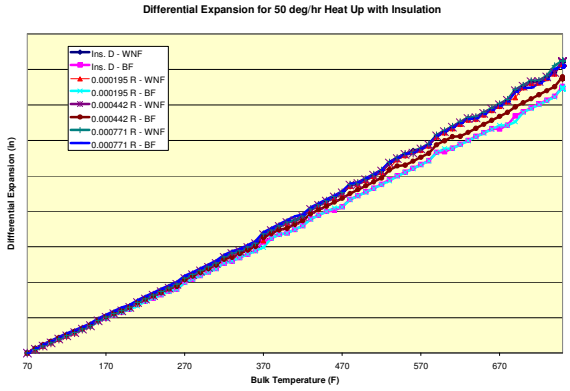

FIGURE 14 – DIFFERENTIAL DISPLACEMENTS FOR 50 °F/hr CASE WITH INSULATION

Figure 15 shows the same data for the 150 °F/hr heat up case.

Copyright © 2010 by ASME

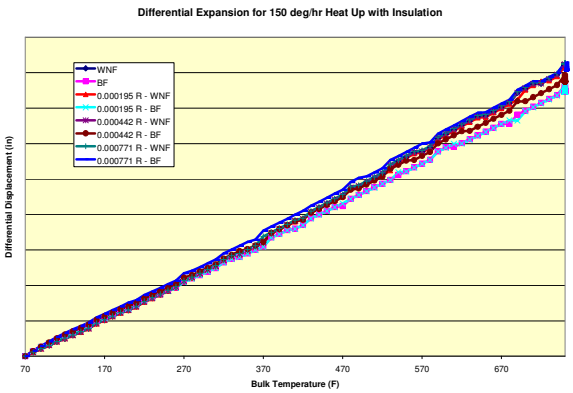

FIGURE 15 – DIFFERENTIAL DISPLACEMENTS FOR 150 °F/hr CASE WITH INSULATION

Figure 16 shows the differential displacements between components for the 50 °F/hr heat up case without insulation.

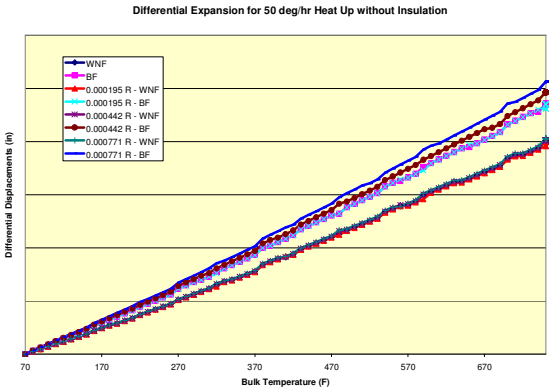

FIGURE 16 – DIFFERENTIAL DISPLACEMENTS FOR 50 °F/hr CASE WITHOUT INSULATION

Figure 17 shows the same data for the 150 °F/hr heat up case.

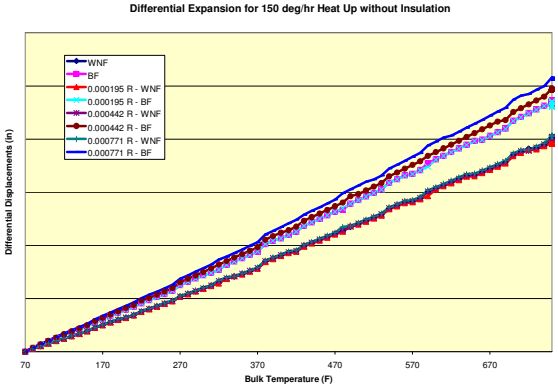

FIGURE 17 – DIFFERENTIAL DISPLACEMENTS FOR 150 °F /hr CASE WITHOUT INSULATION

A comparison of the figures shows that the differential displacements only vary based on the insulation boundary condition; the maximum values for a given insulation state are identical for both heating rates. Also evident from the graphs is the fact that the differential displacements are higher for the uninsulated case than for the insulated case. This result is expected, as the BF should heat up slower and operate at a lower temperature when uninsulated.

Figure 18 contains the temperature differentials between the diaphragm and the WNF and BF versus the bulk temperature for the cases analyzed without insulation.

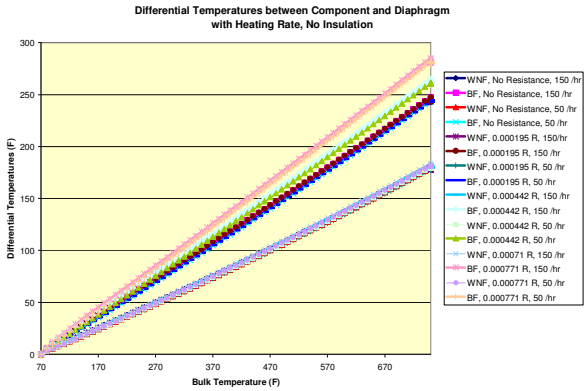

FIGURE 18 – DIFFERENTIAL TEMPERATURES FROM TRANSIENT THERMAL ANALYSES

As can be seen in the figure, the contact resistance does not affect the temperature differential between the WNF and diaphragm. Also evident in the figure is that the temperature differential between the BF and diaphragm follows three lines, corresponding to the different thermal resistances. The 0.000195 hr-ft^2-°F/BTU resistance produced almost the same results as no resistance. The fact that the differential curves are almost identical at both heating rates indicates that heating rate is not significant in the differential temperatures and corresponding strains within the design. Therefore, it can be stated that the maximum differential thermal strain will exist at the exchanger's operational temperature if a reasonable heating rate is maintained during start-up. Steps will be taken during the structural analysis to confirm or deny this statement.

Elastic Structural Analysis

The same axisymmetric model used for the thermal analysis was used for the structural analyses. The thermal contact, previously mentioned, was modified to structural contact. As no public domain data could provide a source for the expected friction coefficient between the diaphragm and flanges (only a maximum value was posited), several values were analyzed, including: no friction, 0.2, 0.4 and 0.6 as the coefficients of static friction. The surface contact type

Copyright © 2010 by ASME

was stick-slip, so no dynamic coefficient of friction was considered. This aids tremendously in model convergence, and with the magnitude of forces occurring in the exchanger should not be an unreasonable assumption.

The properties for both elastic modulus and thermal expansion coefficient were input for the complete temperature range and applied by the software per the temperatures present at the analysis based on tables TM-1 and TE-1 [15]. Figure 19 shows the material properties used for the analysis.

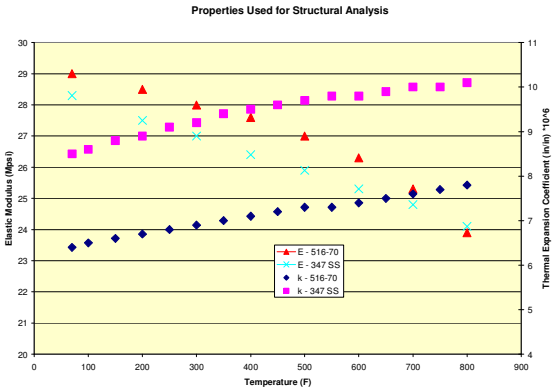

FIGURE 19 – MATERIAL PROPERTIES USED FOR STRUCTURAL ANALYSIS

The analyses were performed using Algor's Nonlinear Static solver [13]. This solver requires time steps to resolve the contact conditions and material properties, but does not include any inertial effects. For evaluation of calculated stresses via Code, all stresses were evaluated as elastic. As the time-scales considered in these analyses are measured in hours, an elastic, non-inertial, stepped analysis with nonlinear contact and temperature dependent properties represents the present state of the art for performing this analysis. Such a methodology allows for the consideration of as many secondary factors as possible in the design analyses.

Under nominal startup operation of such an exchanger there would be a slight pressurization (20% of operating pressure) before heat up occurred. Idealized, then the exchanger's temperature would be linearly ramped from ambient to working while the pressure would also be ramped from 20% to working along a linear curve. This was the case considered during these analyses. The load curve for the exchanger was begun at 20% pressure and ambient conditions. The 20% pressure ensured convergence of the contact conditions in the first step. Options available in Algor mandated that the bolt preload (40% S_y for B7 studs) be applied in the first step. As friction was considered in the analyses, a single step analysis would not produce acceptable results. The structure needed to be allowed to deform along a path dictated by loads. Therefore, a pseudo-time-stepped analysis (per the static analysis) was performed, with 100 steps allowed per thermal/pressure load cycle. With contact included, requiring a nonlinear solution, best practice is to apply the mechanical loads via a versine load curve. A routine was implemented to allow application of the pressure via this curve, while transferring the corresponding temperatures for the static mechanical step to the model.

As initial model convergence dictated the application of the 20% pressure, the load cycle for pressure and temperature was allowed to return to zero to establish the baseline bolt pretension stresses for Code evaluation. Additionally, it was found during the initial analyses that due to the stick-slip conditions included in the model, hysteresis occurred when friction was included in the analysis. For the models demonstrating hysteresis, two load cycles were performed. Figure 20 shows a sample pressure load curve from the analyses.

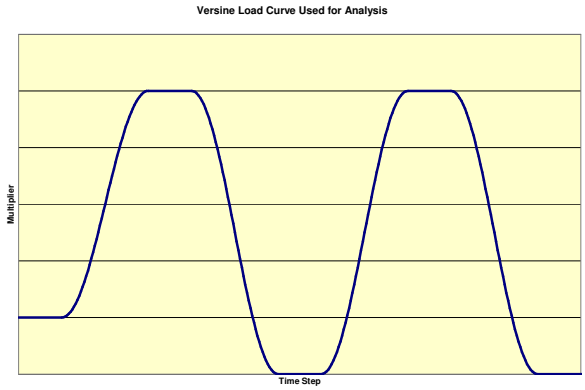

FIGURE 20 – TYPICAL LOAD CURVE USED FOR ANALYSIS

The analyses were allowed to proceed past the second zero load multiplier for 50 steps to ensure steady-state convergence of the model displacements and corresponding stresses at the bolt preload condition.

A second case was considered for emergency shutdown (ESD). In this case the exchanger temperatures were held at steady-state, while the pressure was quickly relaxed to 0 gauge.

Figure 21 shows the typical stress results from a step in the analyses.

Copyright © 2010 by ASME

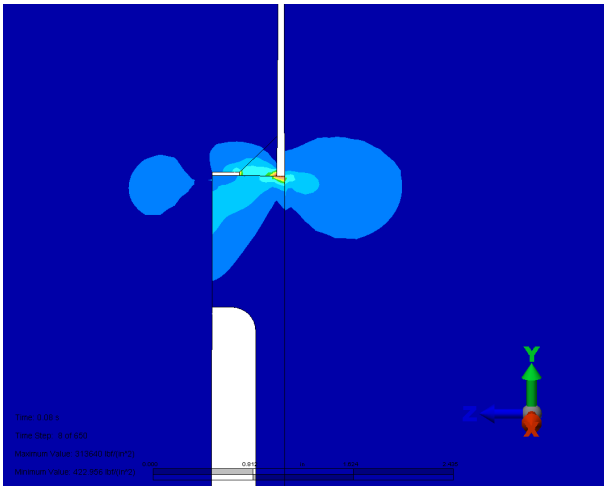

FIGURE 21 – TYPICAL STRESS RESULTS FROM ANALYSES

As can be seen from the figure, the peak stress in the weld occurs at the weld–to-diaphragm OD location and the peak stress in the diaphragm occurs at the periphery where the diaphragm contacts the BF. Therefore, step dependent stresses, σ_{xx}, σ_{yy}, σ_{zz} and τ_{yz} (τ_{xy} and τ_{xz} were 0 due to the axisymmetric assumption) at these two locations were output for Code evaluation. Figure 22 shows typical queried stress results from an analysis.

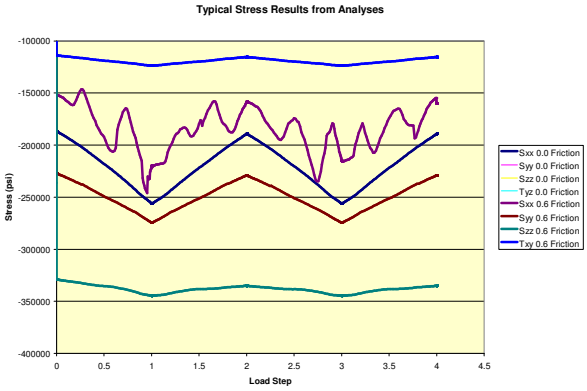

FIGURE 22 – QUERIED STRESS RESULTS FROM ANALYSIS

Assuming the use of 40% of stud minimum yield as the original stud bolt up stress, the linear analysis confirmed that the maximum stud stress did not exceed yield during the thermal cycles analyzed. The 40% of yield bolt up stress in the studs is considered to be sufficient to meet a design for resisting the hydraulic end force during hydrotest while maintaining at least 50% of the Code [6] minimum gasket seating stress.

The stresses indicated in the diaphragm and associated weld exceed the allowable stress values; therefore, an elastic fatigue analysis is required. The procedures used in this analysis are detailed in the **CODE ELASTIC FATIGUE ANALYSIS** Section.

Figure 23 shows the von Mises stress results from the analyses as reported by Algor.

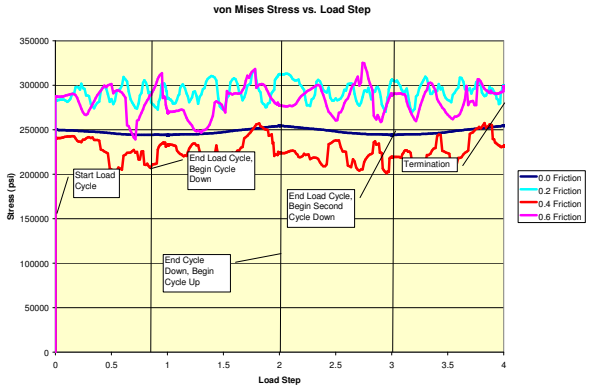

FIGURE 23 – von MISES STRESS RESULTS FROM ANALYSES

As can be seen in the figure, significant hysteresis exists in the system when friction is included. The structure does not return to its preload state. Accommodations for this fact will need to be taken during the 5.5.4 Fatigue Assessment – Elastic-Plastic Stress Analysis and Equivalent Strains Code stress evaluation. As discussed in the **FUTURE WORK** Section, additional analyses will need to be performed to quantify the frictional effects.

Plastic Analysis Results

To confirm the elastic analysis results, it was decided to perform a plastic analysis on the structure. Similar designs have been operated, maintained and inspected over a 20+ year life cycle. From the authors' experience, one would expect no gross deformation (scarring) on the WNF and that plastic strains in the diaphragm should be minimal (< 5%).

To perform the analyses, temperature-dependent yield strengths were defined for the materials [15]. The strain hardening modulus above yield was defined as 5% of the elastic modulus. While this is typically high for most materials, it allows for qualification of the stress results without relying on proprietary information, and also aids convergence.

The model was analyzed with a friction coefficient of 0.6 through the previously described load curves. Querying the maximum von Mises stress results at the preload point in the load curve produces a value of ~80 ksi. Von Mises stress should be used for the queried stresses, as these stresses are used for Algor's yield criteria. Figure 24 contains the results from the plastic analysis.

Copyright © 2010 by ASME

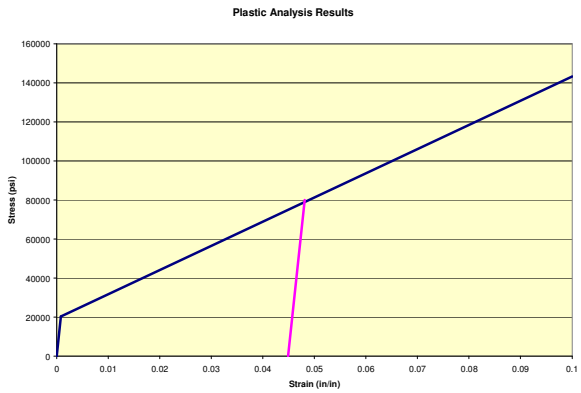

FIGURE 24 – PLASTIC ANALYSIS RESULTS

As can be seen, if the model were unloaded from the final stress condition, there would be less than 5% permanent strain in the diaphragm. Also, there are no residual/permanent strains in the BF or WNF, indicating that no marring would be evident. This step allows confirmation that the model is behaving as would be expected in-service.

CODE ELASTIC FATIGUE ANALYSIS

This section references ASME BVPC Div. 2 2007 [8] for all referenced paragraphs and equation numbers.

Once the stresses had been output for all load cases analyzed, the alternating equivalent stress could be calculated via Paragraph 5.5.3, Equation 5.29. The Code specifies that two time points should be considered. For the case under evaluation, the time points are bolt preload only and the step in the analysis. For models exhibiting hysteresis, the bolt preload stress was established as the stress at the end of each load cycle. Figure 25 shows the stresses calculated for all of the situations considered.

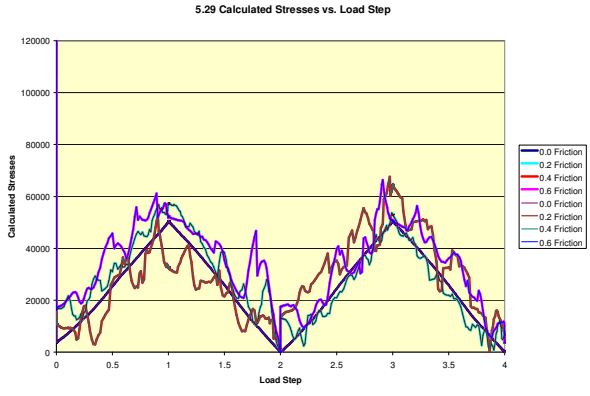

FIGURE 25 – STRESSES CALCULATED via EQUATION 5.29

It should once again be noted that the inclusion of friction significantly affects the calculated results. The results from the low friction, 0.2 static factor case are similar to the no friction results, while it is obvious that significant slip and associated stress spikes occur if friction is dominant for the load- path-determined deformations. Complete evaluation of the design would require evaluation of the movement, with kinematic friction considered, through the slip portions of the load curve. This may be evaluated using the procedures specified in 5.5.4 Fatigue Assessment – Elastic-Plastic Stress Analysis and Equivalent Strains during future work.

Table 5.13 gives factors for Equations 5.31 – 5.33. In this case, m = 1.7 and n = 0.3. $K_{e,k}$ can then be calculated based upon the parameters in the Code. For the stresses calculated in these analyses, Equation 5.33 should be used to calculate the value of $K_{e,k}$, 0.33.

With the definition of $K_{e,k}$, the alternating stress can be calculated using Equation 5.35. This stress can then be used to calculate the expected number of cycles using Equations 3.F.1 and 3.F.2. For this analysis case, the design thermal emergency shutdown cycles are 2 per year for 20 years, and the design thermal normal operation cycles are 5 per year for 20 years. The calculated cycle life indicated a safety factor >10 for emergency and normal thermal cycles.

LESSONS LEARNED / FUTURE WORK

The authors sought to quantify variability due to selected model inputs in the initial analyses that were performed. Along the way, information was acquired that is applicable to future analyses or in-field operations. These are detailed below:

1) CFD Analysis – The CFD analysis was performed to study the convection coefficient in an area where standard information is not available. The results of the CFD analyses produced "design book" values for most coefficients. In areas with reduced flow velocities (such as the passage studied), a value of ½ standard should provide acceptable results. If there exists a flow passage dissimilar to the one studied, or significantly different from "design book" cases, the decision on whether to derive coefficients through CFD is left to the engineer.

2) Other Models – As previously mentioned, other models were used to define the mesh density required. Some of these models contained different weldment and diaphragm dimensions. At low diaphragm widths at the contact between the channel WNF and the diaphragm, the contact pressure on the WNF was found to be excessive. A typical design criteria dictates that the contact stress in the diaphragm ring should not exceed two times the Code [3] minimum yield for the lowest

Copyright © 2010 by ASME

yield material during hydrotest and normal operation. The authors intend to explore this issue further in the future.

3) Insulation – From the results presented in this paper, it is obvious that a BF with insulation does not cause as much differential expansion as a BF without insulation. If an operator believes that a closure (such as studied in this paper) may be subjected to excessive differential expansion conditions, the addition of an insulating blanket on the blind flange not extending to the stud bolts will reduce operating differential expansion and stresses.

4) Material Properties – As mentioned in the paper, at the time of the analyses very limited public domain data was available for the hydrocarbon fluid properties. Since that time, the authors have found a public domain source for dodecane fluid properties as a function of temperature and pressure (Caudwell [16]). While the fluid properties are very similar to the properties used in these analyses, they allow for a more rigorous CFD analysis to be performed. The authors desire to implement these properties into the CFD model to ensure that the calculated coefficients are valid over the entire cycle range. It is expected that the CFD results will not be significantly affected, as the calculated results were similar to standard heat transfer coefficients. If the authors find that significant variation occurs with the complete properties, the results will be reported to the community.

5) Friction – As discussed in the **FEA MODEL** section, the stick-slip assumption is considered to be valid. Time was not available to test complete friction modeling with inertia. Investigation of this may be considered for additional justification in the use of the stick-slip assumption. Additionally, due to the highly nonlinear nature of this process, it would be wise to verify results though the use of at least 2 FE analysis codes. The authors intend to perform this verification.

6) Cycle Count – It is obvious from the results that the model - including friction - is highly nonlinear in response. While the procedures detailed above chose an arbitrary preload state for Code calculations, it is advised that numerous cycles (10+) should be considered in the analysis. Per Code, the baseline, pre-stress state would need to be established and a cycle count would need to be performed for each of the cycles exhibiting hysteresis. Ideally, many analysis cycles run on the frictional models would result in a determinant result for the bolt preload stress case. This stress could then be used to establish operational alternating stresses due to thermal cycles. The authors intend to perform this analysis.

7) Additional Analysis – While the models presented in this paper were adequate to capture the behaviors needed for Code evaluation, they were not refined enough to capture gross deformation at the highly stressed weld location and at the contact between the diaphragm and the BF. All requirements for evaluation via Paragraph 5.5.2, Equation 5.29 were met. It is the authors' intention to also perform evaluation via Equation 5.25 through the implementation of additional load cases. The authors also intend to refine the model and perform Code evaluations as defined in Paragraph 5.5.4, Fatigue Assessment – Elastic-Plastic Stress Analysis and Equivalent Strains to compare to the elastic fatigue results obtained by the procedures reported in this paper. Results will be published to aid in guiding design methodology decisions.

CONCLUSIONS

A procedure including reasonable analysis methodology has been demonstrated for the evaluation of a diaphragm closure. In this instance, for the load cases considered, the diaphragm closure should meet the number of cycles that typically occur in a plant. This analysis result has been confirmed through long-term operation of similar closures.

It should be noted that the authors have only considered two plant operating cases, normal thermal cycle and ESD. In Assessment Procedure 5.5.3.2, Step 1, it is specified that all load histories should be established. Therefore, this paper should not be used as a reference for establishing the complete design suitability of a certain closure. That said, the procedures established in this paper can be used to qualify a specific load history when established, as well as the resulting differential thermal expansion and stress.

It should be noted, as detailed above, that several important assumptions were made in the analyses presented. When any of the assumptions are violated, the procedures specified in this paper may not be valid. Specifically, in the previous paper [1] steps were not taken in the design to minimize thermal variations. It should be noted that in the design considered, steps were taken to ensure that the diaphragm was exposed to a nearly consistent temperature and fluid side process

Copyright © 2010 by ASME

conditions. Care must be taken by the design or analysis engineer to ensure that the axisymmetric assumption is valid.

This paper is presented as a best practice guide based on the information available to the authors. Feedback is sought from the community on modifications to the methodology that could make the analysis more rigorous. The author's goal is to use information developed in future analyses to guide the adoption of a Standard, Methodology for the design of diaphragm closures.

REFERENCES

[1] Porter, M., and Martens, D.H., 2006. Reinvestigation of Heat Exchanger Flange Leak. PVP2006-93731

[2] Porter, M.A., and Martens, D.H., 1994, *Investigation and Repair of Heat Exchanger Flange Leak*, PVP **278**, (Developments in Pressure Vessel and Piping), American Society of Mechanical Engineers., New York, NY

[3] ASME. 2007. 2007 BPVC Section VIII – Rules for Construction of Pressure Vessels Division 2 – Alternative Rules. New York, NY

[4] ASME. 2007. BPVC-VIII – 2007 BPVC Section VIII – Rules for Construction of Pressure Vessels Division I. New York, NY

[5] ASME. 2008. B31.3 – 2008 Process Piping. New York, NY

[6] ASME. 2007. B16.20 – 2007 Metallic Gaskets for Pipe Flanges: Ring-Joint, Spiral Wound, and Jacketed. New York, NY

[7] ASME. 2006. B16.47 – 2006 Large Diameter Steel Flanges: NPS 26 Through NPS 60 Metric/Inch Standard. New York, NY

[8] ASME. 2007. 2007 BPVC Section VIII – Rules for Construction of Pressure Vessels Division 2 – Alternative Rules. New York, NY

[9] CD-Adapco. Star-CCM+. v. 4.06.011. 2009

[10] CD-Adapco. Star-CCM+ User Material Library

[11] MatWeb. ZIRCAR Ceramics Alumina-Silica Insulation

[12] Hodge, B.K. 1990. Analysis and Design of Energy Systems, Second Edition. Prentice-Hall, Inc. Englewood Cliffs, NJ.

[13] Algor. v. 23.1. Build 23.01.00.0136. February 2009

[14] General Electric Heat Transfer Division. 1970. Conduction in Solids – Steady State, Imperfect Metal-To-Metal Surface Contact. Section 502.5. pgs. 1-24

[15] ASME. 2007. 2007 ASME Boiler and Pressure Vessel Code. Section II, Materials. New York, NY

[16] Caudwell, D.R. Trusler, J.P.M., Vesovic, V. and Wakeham, W.A. 2003. The Viscosity and Density of n-Dodecane and n-Octdecane at Pressures up to 200 MPa and Temperatures up to 473 K. NIST

Copyright © 2010 by ASME